Temperature-induced strain and doping in monolayer and bilayer isotopically labeled graphene

T. G. A. Verhagen,[1] K. Drogowska,[2] M. Kalbac,[2,*] and J. Vejpravova[1]

[1]*Institute of Physics of the CAS, v.v.i., Na Slovance 1999/2, CZ-182 21 Prague 8, Czech Republic*

[2]*J. Heyrovsky Institute of Physical Chemistry of the CAS, v.v.i., Dolejskova 2155/3, CZ-182 23 Prague 8, Czech Republic*

(Received 25 November 2014; revised manuscript received 29 May 2015; published 28 September 2015)

The electronic band structure of graphene is strongly dependent on the amount of strain and/or doping present. We performed a comprehensive study of temperature-dependent strain and doping in isotopically labeled graphene mono- and bilayers on a SiO_2/Si substrate by Raman spectral mapping at well-defined temperatures between 300 and 10 K. The principal Raman active modes of the graphene (G, 2D) were subjected to correlation analysis, which enabled reliable separation of the strain and doping contributions. The influence of strain on the monolayer and top and bottom layers of the bilayer graphene is large and shows a pronounced temperature-dependent variation. A clear difference is observed in local strain fluctuations on length scales much smaller than the laser spot. In both the monolayer and the bottom layer of the bilayer, which are in contact with the substrate, a significant amount of local strain is induced when the temperature is varied. In contrast, the influence of local strain on the top layer of the bilayer is much smaller. Temperature dependence of the doping is clearly present in both layers, suggesting equalization of the captured charge in the bilayer down to low temperatures.

DOI: 10.1103/PhysRevB.92.125437 PACS number(s): 78.30.−j, 63.22.Rc, 81.05.ue

I. INTRODUCTION

Graphene, a monolayer graphite sheet consisting of sp^2-hybridized covalently bonded carbon atoms, has shown many useful electronic [1,2], optical [3,4], plasmonic [5], mechanical [6], and thermal [7] properties, which has led to numerous proposals of unique graphene-based applications [8]. Many of them rely on control of the electronic band structure, which can be efficiently modulated via either doping or strain [1,9–13].

When graphene mono- and bilayers are placed on a substrate, the interaction between them plays an important role in the doping and strain of the graphene layer and thus also in the changes of the electronic band structure. It is well known that the interaction between graphene and a SiO_2/Si substrate induces unintentional and inhomogeneous doping due to charged impurities [14,15], which can be clearly identified by a shift of the Dirac point [1,9].

Furthermore, the graphene layer adapts to the structure of the underlying substrate, which results in microscopic corrugations [16–19]. These corrugations induce a certain amount of compressive and/or tensile stress locally, which can lead to strain-induced pseudomagnetic fields causing discretization of the graphene band structure without an external magnetic field [10,20]. In bilayer graphene, the topology of the low-energy band structure critically depends on mechanical deformations of the two-dimensional crystal, as the strain determines the number of Dirac cones in the low-energy part of the spectrum [12,13].

During the chemical-vapor-deposition growth of graphene on metals such as Cu [21] or Pt (111) and Ir (111) [22], the annealing steps after the transfer of graphene to a SiO_2/Si substrate, and, finally, the low-temperature measurement, the mismatch between the thermal expansion coefficient (TEC) of graphene and the TEC of the substrate will induce extra thermal contraction/expansion of the graphene when the sample is heated [23] or cooled [24]. It is expected that these large temperature variations (measurements at millikelvins, annealing at 800 K, and growth at 1273 K) and repeated temperature cyclings will drastically modify the strain and doping present.

Obviously, the temperature-induced interaction of the graphene with the substrate and/or mutual interaction of the layers lead to changes in the band structure and hence play an important role in the correct interpretation of the transport properties. Whereas induced doping can be effectively compensated via gating of the structure, it is very difficult to compensate the strain induced on graphene. For the correct interpretation of low-temperature transport measurements, it is then of utmost importance to know how the strain of the graphene layer changes when the sample is cooled.

Raman spectroscopy is a useful tool for the study of graphene, as the two most important processes that contribute to a change in the Raman shift of the G and 2D modes of graphene are the strain and the doping [25–28]. Das *et al.* [25,26] showed that electron and hole doping leads to a change in the Raman shift of the G and 2D modes. However, also a small amount of compressive or tensile strain [27,28] leads to a moderate change in the Raman shift in the G and 2D modes.

Lee *et al.* [29] recently showed that the contributions of mechanical strain and charge doping to the Raman spectra of graphene can be distinguished from each other using a correlation analysis of the two dominant modes in the graphene Raman spectra, the G and 2D modes. Using this approach, they concluded that a substantial change in the strain and doping level occurs when a graphene sample is annealed at temperatures varying between 373 and 773 K.

Recently, different groups have also studied the low-temperature dependence of the Raman shift of the G and 2D phonon modes of graphene and graphite [24,30–33]. The behavior of the Raman shift of the G and 2D modes can be attributed to two major effects: the temperature dependence of the phonon anharmonicity and the different and opposite TECs of the graphene and the substrate, which induce strain.

*martin.kalbac@jh-inst.cas.cz

The anharmonic phonon effect is a combined effect of electron-phonon and phonon-phonon interactions and plays a key role in material properties such as specific heat, thermal expansion, and carrier transport properties. The influence of the phonon anharmonicity of graphene on the line widths and wave numbers of the phonon modes has been calculated by Bonini *et al.* [32].

To date, the low-temperature dependence of Raman spectra has been studied by following a single spot on a graphene flake. Unfortunately, with this type of measurements, it is impossible to keep the laser spot at exactly the same place when varying the temperature. A slightly different position of the laser spot can result in a different Raman spectrum of graphene. This can be caused by a different contact of the graphene with the substrate, local strain and doping variations, or the presence of the edge of a graphene flake or domain of the graphene grown by chemical vapor deposition. Therefore, it is more reliable to analyze Raman maps of the area of interest, which will provide sufficient statistics to draw conclusions.

Furthermore, the development of isotope labeling of graphene bilayers [34,35] makes it possible to follow the Raman spectra of the bottom and top layers independently. This enables us to distinguish between the interaction of the graphene bottom layer with the substrate and the interaction of the graphene top layer with the graphene bottom layer.

In this paper, we present measurements of low-temperature-dependent Raman spectral mapping of isotopically labeled graphene mono- and bilayers. By following the same area of the graphene sheet, we are able to follow how the properties of the graphene change as a function of the temperature. The large number of spectra collected in a Raman map allows us to use the correlation analysis proposed by Lee *et al.* [29] to distinguish the influence of both the strain and the doping on the Raman shift of the principal modes of graphene.

In the first part of this paper, we introduce the sample preparation, the experimental setup for low-temperature Raman spectral mapping, and the method for analysis of the Raman maps. In the second part of the paper, the behaviors of the monolayer and bilayer graphene areas are discussed separately. For both mono- and bilayer graphene, first the temperature dependence of the Raman spectral parameters is shown, and then the temperature-induced strain and doping are discussed.

We find that the influence of strain on monolayer graphene and the bottom and top layers of bilayer graphene is large and shows a significant temperature dependence. Furthermore, when the sample is cooled, strain on length scales much smaller than the laser spot is induced in the graphene layer, which is in contact with the substrate.

The influence of temperature-induced doping is clearly present in both the graphene monolayer and the bottom and top layers of the graphene bilayer.

II. EXPERIMENTAL METHODS

Graphene samples were synthesized by chemical vapor deposition, as reported previously [23]. A copper foil was heated to 1273 K and annealed for 20 min under a flow of 50 standard cubic centimeters per minute (sccm) H_2. Subsequently, it was exposed to 3 sccm $^{12}CH_4$ for 3 min, whereafter the $^{12}CH_4$ was turned off and then the copper foil was exposed to a flow of 3 sccm $^{13}CH_4$ for 20 min. Finally, the sample was cooled to room temperature. Consequently, small islands of ^{12}C graphene with small ad-layers were first grown at the nucleation points. When switching the gas supply from $^{12}CH_4$ to $^{13}CH_4$, the graphene continues to grow, but now containing ^{13}C. Also, the ad-layers continued to grow, but at a lower rate, forming a bilayer of $^{12}C/^{13}C$ graphene. The as-grown graphene was subsequently transferred to a clean SiO_2/Si substrate using poly(methyl methacrylate) (PMMA), according to procedures reported previously [36]. Residual PMMA was removed by thermal annealing at 798 K for 2 h in an Ar/H_2 atmosphere.

The sample was mounted on a low-temperature confocal Raman microscope insert (attoRAMAN, attocube), which was placed in a Physical Property Measurement System (PPMS; Quantum Design). This configuration guarantees very stable experimental conditions. The sample space was flushed several times with He gas to ensure stable doping, whereafter the sample space was evacuated to 5 mbar. Raman spectra were acquired using a WITec Alpha300 spectrometer with 2.33-eV (532-nm) laser excitation, a grating of 1200 lines/mm, a 100× objective (numerical aperture, 0.82), a laser spot diameter on the sample of slightly better than 500 nm [37] and a lateral resolution of 500 nm. The sample was subsequently cooled from 300 to 10 K, where the sample temperature was monitored with a thermometer placed just below the sample. A Raman map of approximately the same sample area of $25 \times 25\ \mu m^2$ was acquired every 50 K, with lateral steps of 500 nm in both directions. Spectra were collected using a laser power of approximately 1 mW and an accumulation time of 26 s. After the low-temperature experiment, the sample was fluorinated [38,39] to address the stacking orientation of the ^{12}C and ^{13}C graphene layers.

To analyze all of the spectra, we fit each of them as shown in Fig. 1(a). First, a linear background was subtracted from an interval around the Raman peaks. Thereafter the peaks were fitted with a pseudo-Voigt peak function. A pseudo-Voigt peak function is a linear combination of a Gaussian and a Lorentzian function, where the Gaussian function describes the broadening of a Lorentzian peak. The Raman intensity is then given by

$$\begin{aligned}&\text{Raman intensity}(I,\omega,\omega_0,\Gamma,\alpha)\\&= (1-\alpha)I\sqrt{\frac{\ln 2}{4\pi\Gamma^2}}\exp\left(\frac{-\ln 2(\omega-\omega_0)^2}{4\Gamma^2}\right)\\&\quad+\alpha\frac{I}{2\pi\Gamma}\cdot\frac{1}{1+\frac{(\omega-\omega_0)^2}{4\Gamma^2}},\end{aligned}\tag{1}$$

where Γ is the full width at half-maximum (FWHM), I the peak intensity, ω the Raman shift, ω_0 the position of the Raman peak, and α the fraction of the peak that is Lorentzian.

Because of the huge temperature variations the sample has experienced during the sample growth [21,22], annealing, and final low-temperature measurements, wrinkles are present. At the wrinkle, the graphene is locally "lifted" from the substrate or the bottom graphene layer, and hence it feels a locally different strain and doping level. As a result, a bimodal

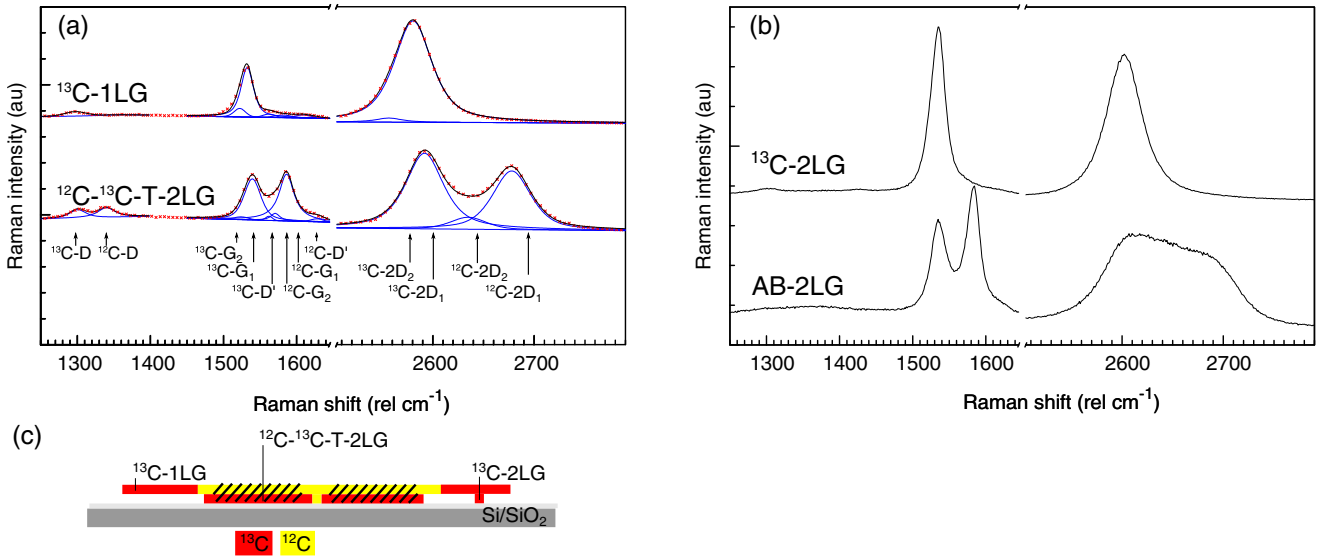

FIG. 1. (Color online) (a) Typical Raman spectra of a ^{13}C single-layer graphene (^{13}C-1LG) and a ^{12}C-^{13}C turbostratic stacked bilayer graphene (^{12}C-^{13}C–T-2LG) are shown at 300 K. The (red) x's represent the experimental data and solid black lines are the convoluted pseudo-Voigt line shapes used to fit the data. Blue lines correspond to the individual G_1, G_2, and D′ peaks of the G mode and $2D_1$ and $2D_2$ components of the $2D_2$ mode, respectively. Spectra are offset for clarity. (b) Typical Raman spectra at 300 K of a ^{13}C bilayer graphene (^{13}C-2LG) and a ^{12}C-^{13}C Bernal-stacked bilayer graphene (AB-2LG), which are also present in the sample. (c) Scheme of the layer orientation as a cross section through a grain. The hatched region within the ^{12}C-^{13}C island indicates the region where the ^{12}C-^{13}C–T-2LG can be found.

distribution of doping and strain is observed; the graphene is either in contact with the substrate or lifted from the substrate in the wrinkled region [40,41].

We fit, therefore, the ^{12}C-D peak with a single pseudo-Voigt line shape, the ^{12}C-G peak with three pseudo-Voigt line shapes (^{12}C-G_1, ^{12}C-G_2, and a ^{12}C-D′), and the ^{12}C-2D peak with two pseudo-Voigt line shapes (^{12}C-$2D_1$ and ^{12}C-$2D_2$). The ^{12}C-G_1 and ^{12}C-$2D_1$ peaks account for the behavior of the graphene layer that is in contact with the substrate/bottom layer and the ^{12}C-G_2 and ^{12}C-$2D_2$ peaks account for the graphene layer that is lifted from the substrate/bottom layer in the laser spot area [40,41]. Simultaneously, the same procedure is used to fit the ^{13}C-isotope peaks. In the remainder of this paper, the G_1 and the $2D_1$ peaks are used to study the global behavior of the graphene layer.

To compare the Raman spectra at different temperatures, the same area of the Raman map was extracted at each temperature. In Fig. 2, the maps of the intensity of the ^{12}C and ^{13}C G_1 mode are shown for each temperature.

Isotope labeling is used to follow the behavior of the bottom and top layers of the graphene bilayers independently. The higher mass of the ^{13}C isotope with respect to the ^{12}C isotope

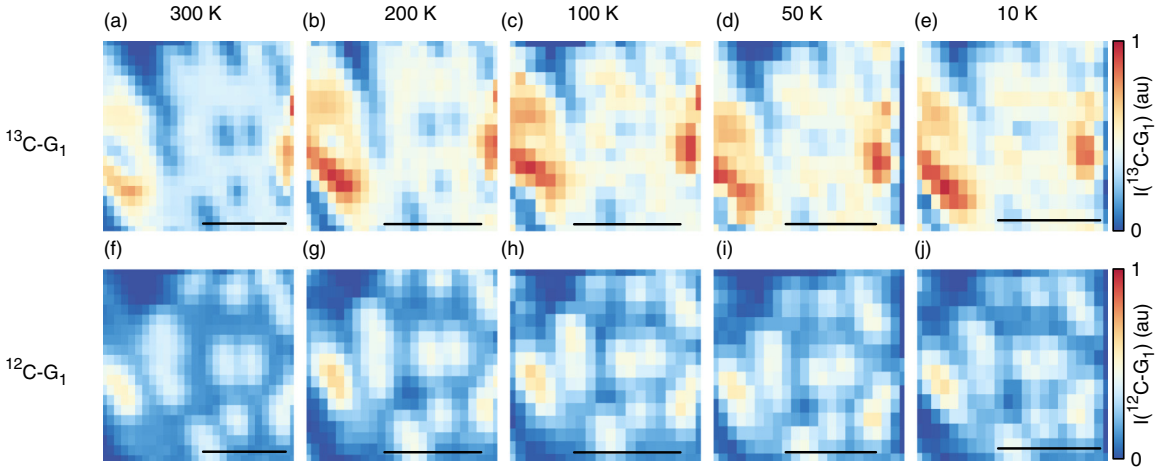

FIG. 2. (Color online) Raman maps of the fitted peak intensity in arbitrary units for the G_1 mode for the ^{13}C (upper row) and ^{12}C (lower row) isotopes, measured at 300 K (a, f), 200 K (b, g), 100 K (c, h), 50 K (d, i), and 10 K (e, j). The dimensions of the Raman maps at different temperatures are slightly different, but the scale bar in each panel is 5 μm.

results in a downshift of the Raman shift equal to

$$\frac{\omega_{12}-\omega_{13}}{\omega_{12}} = 1 - \sqrt{\frac{12+c_0^{13}}{12+c_{13}^{13}}}, \qquad (2)$$

where ω_{12} and ω_{13} are the Raman shifts of the ^{12}C- and ^{13}C-enriched samples, respectively. c_0^{13} is the natural abundance of ^{13}C in the graphene grown with the $^{12}CH_4$ precursor, which is equal to 0.0107. c_{13}^{13} is the purity of the ^{13}C in the enriched sample, usually determined by the isotope purity of the $^{13}CH_4$ precursor (here $c_{13}^{13} = 0.99$).

III. RESULTS

Figures 2(a) and 2(f) show Raman maps at 300 K of the fitted peak intensity of the G_1 mode for the ^{13}C and ^{12}C isotopes. It is clearly visible that growth starts with the formation of small ^{12}C graphene islands. When the precursor gas is switched to $^{13}CH_4$, the growth continues. As recently shown by different groups [38,39,42], the second ^{13}C graphene layer grows below the first ^{12}C graphene layer. Using the fluorination method [38,39], we confirmed that this is also the case for the sample shown in Fig. 2.

For the studied samples, a full coverage has not been obtained, which helps to identify a particular spot. In these maps, ^{13}C (^{13}C-1LG) monolayer graphene areas (more than 200 spectra present at most temperatures) and different types of bilayer graphene—turbostratic stacked bilayer (T-2LG) ^{12}C-^{13}C graphene (more than 100 spectra at each temperature), Bernal-stacked bilayer ^{12}C-^{13}C graphene (AB-2LG), and ^{13}C (^{13}C-2LG) turbostratic stacked bilayer graphene—can be found. Typical Raman spectra are presented in Figs. 1(a) and 1(b), and in Fig. 1(c) the scheme shows the location of the ^{12}C-^{13}C bilayer in the grain. As shown in Fig. 2, there are many more spectra that contain a clear signal of the ^{13}C isotope. As shown in Figs. 1(a) and 2, there is sometimes also a (very) weak signal of the ^{12}C isotope present, which originates from small ^{12}C graphene islands that are much smaller than the laser spot.

It is hardly possible to distinguish the behavior of the top and bottom layers of the ^{13}C-2LG, therefore we focus on the ^{12}C-^{13}C-T-2LG. Here, the temperature dependence of the top and bottom layers of the bilayer graphene can be addressed separately. (We do not include AB-2LG in our analysis, as we have only one spectrum present at each temperature.)

To simplify the discussion of the results, all Raman shifts of the ^{13}C isotope are recalculated using Eq. (2). Furthermore, a statistical analysis of the Raman shifts and FWHM as a function of the temperature has been made. Each data point in Figs. 3–6 is the second quartile (median) of the data set and the "error" bars represent the first and third quartiles.

We prefer to use quartiles, instead of the commonly used mean value with its standard deviation, because the distribution of the fitted data is often skewed and not normally distributed, as clearly shown in recent work by Frank *et al.* [43] and Ek Weis *et al.* [39] (see Supplemental Material [37] for a comparison between the two methods for ^{13}C-1LG at 300 K). Furthermore, quartile statistics takes outliers better into account, which are often encountered in large Raman maps.

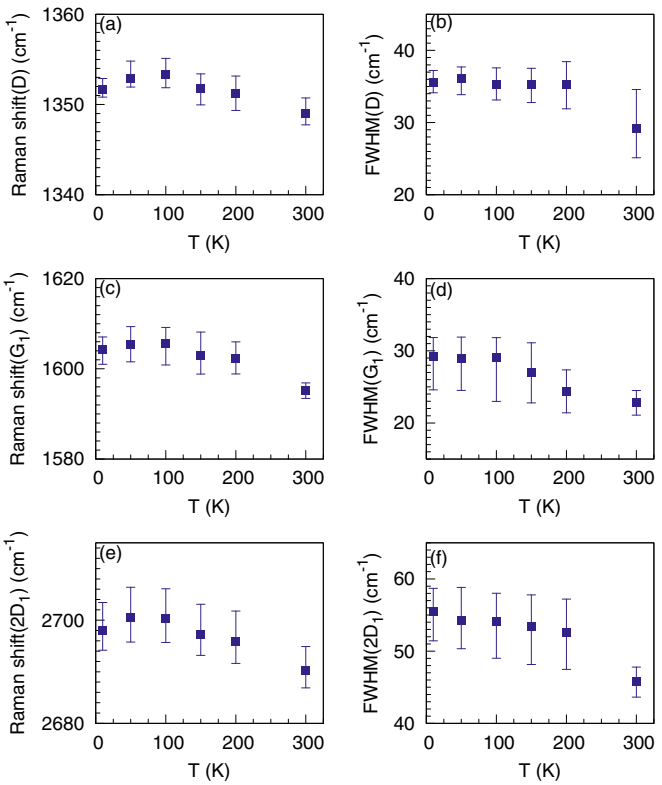

FIG. 3. (Color online) Temperature dependence of the median Raman shift, and median FWHM of the D mode (a, b), the G_1 mode (c, d), and the $2D_1$ mode (e, f) for ^{13}C-1LG. "Error" bars represent the first and third quartiles of each data set. Raman shifts from ^{13}C-1LG are recalculated via Eq. (2) to be comparable with ^{12}C graphene.

A. Monolayer

In this section, the temperature dependence of ^{13}C-1LG is discussed. Figure 1(a) shows a Raman spectrum of a typical ^{13}C-1LG, where the peak intensity of the 2D band of the graphene monolayer is higher than the peak intensity of the G band.

The temperature dependence of the median Raman shifts and median FWHM of the D, G_1, and $2D_1$ peaks obtained for the ^{13}C-1LG are shown in Fig. 3. Figure 3(a) shows that the median Raman shift of the D mode is 1349 cm^{-1} [recalculated via Eq. (2)] at 300 K. When the temperature is decreased from 300 to 100 K, the median Raman shift of the D mode increases continuously; when the temperature is decreased from 100 to 10 K, the median Raman shift decreases. As shown in Fig. 3(b), the median FWHM of the D mode is 29 cm^{-1} at 300 K. The median FWHM increases when the sample is cooled to 200 K and it stays constant when the sample is cooled further to 10 K.

The median Raman shifts of the G_1 and $2D_1$ peaks, as shown in Figs. 3(c) and 3(e), are 1595 and 2690 cm^{-1} [recalculated via Eq. (2)] at 300 K, respectively. When the temperature is decreased from 300 to 100 K, the medians of the Raman shifts of both the G_1 and the $2D_1$ peaks increase. When the temperature is decreased from 100 to 10 K, the median Raman shift decreases by 2 and 3 cm^{-1} for the G_1 and $2D_1$ modes, respectively.

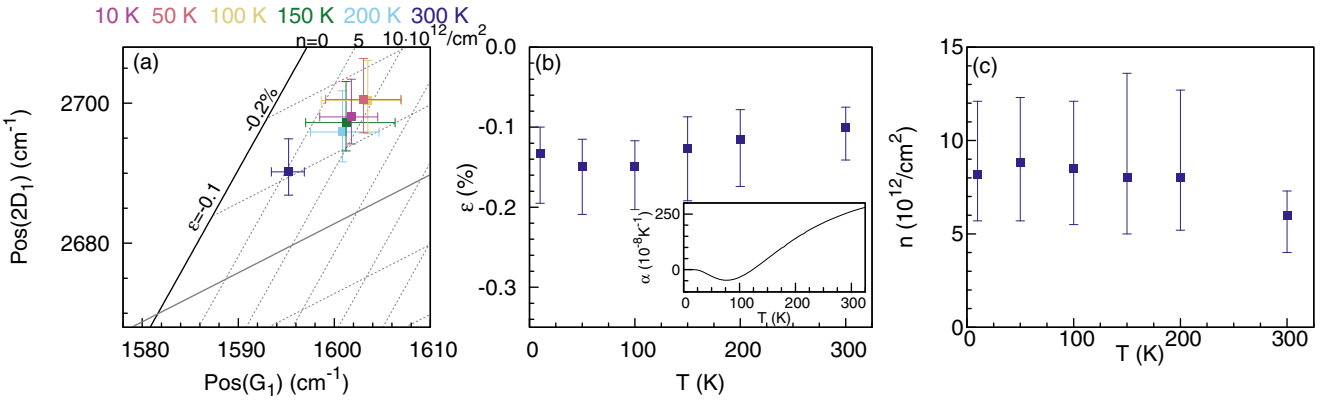

FIG. 4. (Color online) (a) Temperature dependence of the correlation between the median Raman shift of the G_1, Pos(G_1) and $2D_1$, Pos($2D_1$) modes of the spectra of the monolayer (color-coded filled squares). The color code used for the different temperatures is shown above (a). The solid black line indicates pure strain (ϵ) variation, with a slope of 2.45, and the solid gray line indicates pure doping (n) variation, with a slope of 0.7. The temperature dependence of the strain (b) and doping (c) of 1LG derived from (a). Inset in (b): The linear thermal expansivity α of Si, measured by Lyon *et al.* [44], is shown as a reference. Each data point represents the second quartile (median) and "error" bars represent the first and third quartiles of each data set. Raman shifts from ^{13}C-1LG are recalculated via Eq. (2) to be comparable with ^{12}C graphene.

The median FWHM of the G_1 and $2D_1$ modes of ^{13}C-1LG are shown in Figs. 3(d) and 3(f). The median FWHM values of the G_1 and $2D_1$ modes are 23 and 46 cm^{-1} at 300 K, respectively. The median FWHM of both modes increases when the sample is cooled from 300 to 100 K. The median FWHM of the G_1 mode stays constant when the sample is cooled further to 10 K and the median FWHM of the $2D_1$ mode increases when the sample is cooled from 50 to 10 K.

B. Temperature dependence of strain and doping in a monolayer

To investigate the temperature dependence of the strain and doping, we use the correlation analysis proposed by Lee *et al.* [29]. In Fig. 4(a) the correlation between the median Raman shift of the $2D_1$ mode, Pos($2D_1$), and the median Raman shift of the G_1 mode, Pos(G_1), is shown for all temperatures.

Previous Raman spectroscopy studies on graphene have shown that when biaxial strain is applied to undoped graphene, the Raman shift of the G_1 and $2D_1$ modes increases or decreases along one line (the "strain line") in the Pos(G_1) − Pos($2D_1$) phase space, which is indicated by the solid black line in Fig. 4(a) and has a slope ΔPos($2D_1$)/ΔPos(G_1) of 2.45 [28]. When the strain is kept constant, but the doping level is varied, the same behavior can be observed, except that the slope of the "doping line" is different. The doping line is indicated in Fig. 4(a) by the solid gray line and has a slope ΔPos($2D_1$)/ΔPos(G_1) of 0.7 [25]. When the contribution of the strain and doping on the Raman shift is known, the strain and doping of each point in the Pos(G_1)-Pos($2D_1$) space can be deduced.

Each point in the Pos(G_1)-Pos($2D_1$) space can thus be described as a linear combination of the unit vectors of strain e_ϵ and doping e_n. The origin of this coordinate system corresponds to the Raman shifts of a freestanding graphene sheet, which is almost strain- and doping-free. A freestanding graphene sheet has a Raman shift of 1582 cm^{-1} for the G mode and 2677 cm^{-1} for the 2D mode at a laser excitation of 2.41 eV [29]. Because of the dispersive behavior of the 2D mode, the Raman spectrum of the 2D mode changes as a function of the incident laser energy E_l, by approximately 88 cm^{-1}/eV for a graphene monolayer [45,46], whereas dPos(G)/dE_l is small [43]. The origin for excitation with 2.33 eV corresponds to approximately (1582 cm^{-1}, 2670 cm^{-1}).

For low charge-carrier concentrations, the shift in Pos(2D) is negligible compared with the change in Pos(G) as a function of the doping level. The doping level can then be determined from the positive shift ΔPos(G) of the Pos(G) from the strain line [see Fig. 4(a)]. ΔPos(G) can be related to the charge concentration n by approximating the data of Das *et al.* [25] by a quadratic polynomial, $\Delta\text{Pos(G)} = -0.274n^2 + 14.25n$, where n is the charge concentration (in 10^{13}/cm^2). The strain can be estimated from the shift of Pos(2D) from the doping line. Zabel *et al.* [28] showed that the biaxial strain sensitivity of the G mode is equal to –57 cm^{-1}/1%.

When the temperature of graphene is varied, the influence of the phonon anharmonicities changes. This results in a change in the Raman shift of the G and 2D modes, as shown by Bonini *et al.* [32]. As all the experiments to determine the influence of strain and doping on Raman shifts are done at 300 K, we need to correct our data for the influence of phonon anharmonicities. We correct the Raman shifts at all temperatures in Figs. 4 and 6 for the extra Raman shift of the G mode due to phonon anharmonicities, ΔPos(G_{an}), by subtracting the theoretically predicted shift, as calculated by Bonini *et al.* [32]. The contribution of the anharmonic phonon contribution ΔPos(G_{an}) is obtained by approximating the predicted shift of Bonini *et al.* [32] by a third-order polynomial, $\Delta\text{Pos}(G_{an}) = -4.23 \times 10^{-4}\ T - 3.03 \times 10^{-5}\ T^2 + 1.15 \times 10^{-8}\ T^3$, where T is the temperature (in K). We do not correct the 2D mode for the anharmonic phonon contribution, as the change in the Raman shift of the 2D mode in the temperature range 0–300 K is small (about 2 cm^{-1}) compared with the Raman shift induced by doping and strain [47].

The data points in Fig. 4(a) are located somewhere between the strain and the doping lines, which suggests that both strain and doping are present in ^{13}C-1LG. Figure 4(b) shows that

at 300 K the value of the strain is negative, which indicates that there is compressive strain. When cooling the 1LG to 100 K, the strain slowly decreases. If the temperature is decreased further, to 50 K, the strain stays almost constant, and it increases again when it is cooled to 10 K. However, the temperature dependence of the doping shows a different behavior, as shown in Fig. 4(c). When the temperature is decreased from 300 to 200 K, an increase in the doping level can be observed. Further cooling of the sample, to 10 K, does not produce a further increase in doping.

C. Bilayer

Figure 1(a) shows the Raman spectrum of ^{12}C-^{13}C–T-2LG. As the bilayer graphene in Fig. 1 consists of a ^{13}C bottom and a ^{12}C top layer (we denote the bottom layer ^{13}C–T-2LG and the top layer ^{12}C–T-2LG), both the G and the 2D peaks of the ^{12}C and ^{13}C isotopes can now be observed.

Figures 5(a)–5(f) show the temperature dependence of the Raman shift and FWHM of the D, G_1, and $2D_1$ modes of the bottom ^{13}C and top ^{12}C layers of T-2LG. Both the ^{13}C bottom and the ^{12}C top layers show similar behavior as observed for ^{13}C-1LG. When the sample is cooled from 300 to 100 K, an increase in the Raman shift of the G_1 and $2D_1$ modes can be observed and a small decrease in the Raman shift is observed when the sample is cooled from 100 to 10 K.

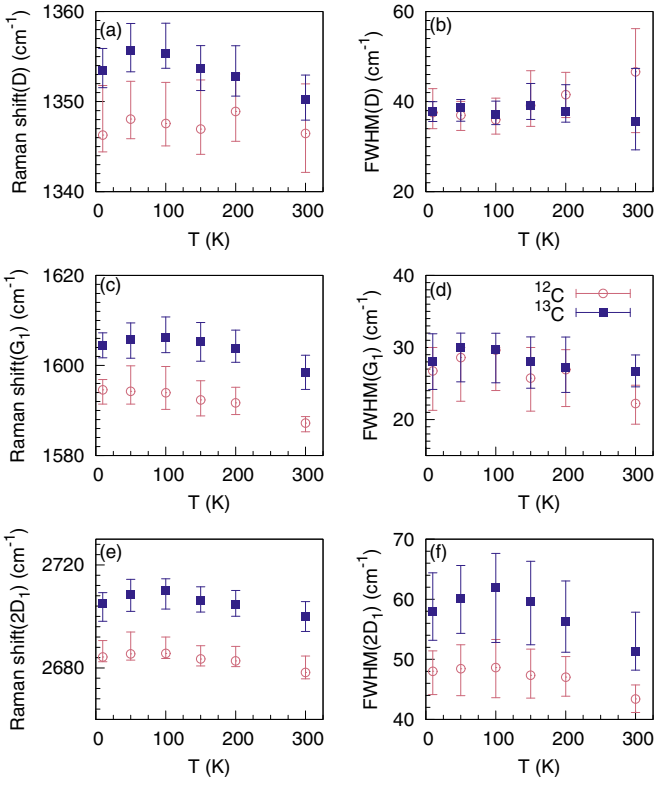

FIG. 5. (Color online) Temperature dependence of the median Raman shift and median FWHM of the D (a-b), G_1 (c-d) and $2D_1$ (e-f) modes of the ^{12}C top [^{12}C–T-2LG; open (red) circles] and ^{13}C bottom layers [^{13}C–T-2LG; filled (blue) squares] of T-2LG. "Error" bars represent the first and third quartiles of each data set. Raman shifts from the ^{13}C bottom layer are recalculated via Eq. (2) to be comparable with the ^{12}C top layer.

The median Raman shift of the G_1 mode at 300 K is equal to 1587 cm^{-1} for the ^{12}C top layer and 1598 cm^{-1} [recalculated via Eq. (2)] for the ^{13}C bottom layer. However, the median Raman shifts of the D modes, which are equal to 1347 cm^{-1} for the ^{12}C layer and 1350 cm^{-1} [recalculated via Eq. (2)] for the ^{13}C layer, do not suggest that the c_{13}^{13} concentration deviates from the expected value.

The temperature dependence of the median FWHM of the G_1 and $2D_1$ modes of the bottom and top layers all show the same trend. When the temperature is decreased from 300 to 100 K, the median FWHM of both modes increases. A small decrease is observed when the temperature is decreased to 10 K. The FWHM of the $2D_1$ modes in Fig. 5(f) shows a difference. The median FWHM of the ^{13}C bottom layer is slightly larger, at 300 K. When the temperature is decreased, the median FWHM of the ^{13}C layer increases more than the median FWHM of the ^{12}C layer.

The correlation between the median Pos(G_1) and the median Pos($2D_1$) is shown in Fig. 6(a). We use the same parameters to analyze the correlation analysis that we used for the ^{13}C monolayer. From Fig. 6(a), we can derive both the strain and the doping level in the bottom and top layers.

Figure 6(a) shows the same trend as observed in Fig. 4(a); both strain and doping are present in the bilayer. In Fig. 6(b) it is clearly visible that there is much more strain present in the ^{13}C bottom layer than in the ^{12}C top layer. However, the strain of the ^{12}C top layer shows a similar variation as that of the ^{13}C bottom layer when the sample is cooled from 300 to 10 K. The strain in both layers decreases when the sample is cooled from 300 to 100 K. When the sample is cooled further, to 10 K, the strain of both the ^{13}C bottom layer and ^{12}C top layer increases again.

The doping level of the ^{13}C bottom layer, as shown in Fig. 6(c), increases when the temperature is decreased from 300 to 200 K, whereafter it decreases again when the sample is cooled to 50 K. Finally, when the sample is cooled to 10 K, the doping level increases slightly again. The doping level of the ^{12}C top layer stays almost constant when the sample is cooled from 300 to 50 K, whereafter it increases when the sample is cooled to 10 K. Furthermore, the doping level of the ^{13}C bottom layer is much larger than the doping level of the ^{12}C top layer.

IV. DISCUSSION

The temperature dependences of the median Raman shift of the G and 2D modes, which are shown in Figs. 3 and 5, of ^{13}C-1LG and T-2LG show no significant difference; an increase in the median Raman shift of the G_1 and $2D_1$ modes is observed when the sample is cooled from 300 to 100 K, and when the temperature is decreased further, the median Raman shift slightly decreases. This behavior is in agreement with experimental results obtained before and can be explained well using the phonon anharmonicities as shown by Bonini *et al.* [32].

From the correlation analysis, which is shown in Figs. 4 and 6, the temperature dependence of the strain and doping level could be determined and a few remarkable features are observed when the correlation analysis is compared among the graphene species. The presence of a small D′ peak in graphene does not lead to any significant change in the Raman shift or

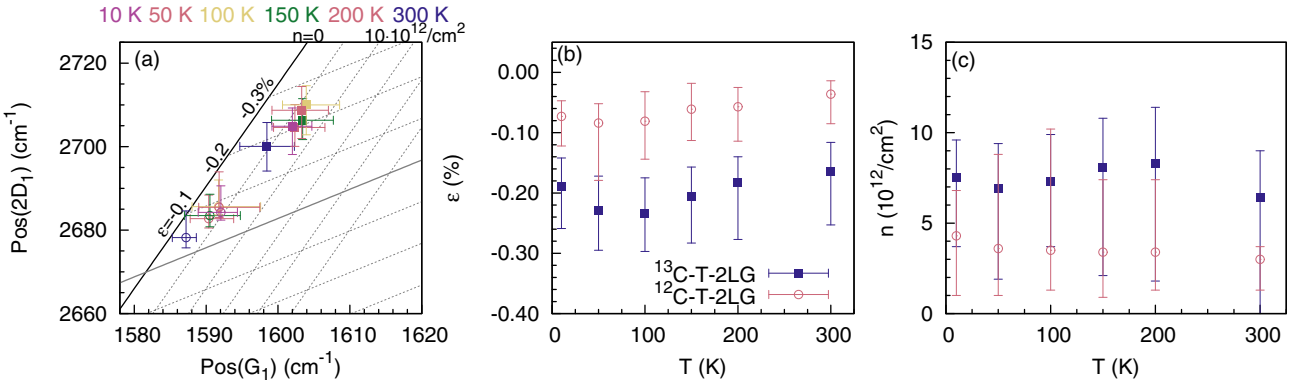

FIG. 6. (Color online) (a) Temperature dependence of the correlation between the median Raman shift of the G_1, $Pos(G_1)$ and $2D_1$, $Pos(2D_1)$ modes of the spectra of ^{13}C–T-2LG (color-coded filled squares) and ^{12}C–T-2LG (color-coded open circles). Raman shifts of the ^{13}C isotope are recalculated via Eq. (2) to be comparable with the Raman shift of the ^{12}C isotope. The solid black line indicates pure strain (ϵ) variation, with a slope of 2.45, and the solid gray line indicates pure doping (n) variation, with a slope of 0.7. The color code used for different temperatures is shown above (a). The temperature dependence of the strain (b) and doping (c) of ^{13}C–T-2LG [filled (blue) squares] and ^{12}C–T-2LG [open (red) circles] derived from (a). Each data point represents the second quartile (median) and "error" bars represents the first and third quartiles of each data set.

broadening of the G or 2D modes [48,49], which suggests little or no change in the doping or strain of the graphene sample due to defect creation.

First, the temperature dependence of the strain in ^{13}C-1LG is not linear as a function of temperature, but a clear minimum in the strain can be observed between 50 and 100 K. The TEC of graphene is negative and opposite the TEC of the SiO_2/Si substrate [24]. The mismatch of the TECs between graphene and substrate will induce a thermal contraction (expansion) of the graphene when the sample is heated (cooled). The induced strain is proportional to the difference between the TEC of graphene and that of SiO_2/Si. As the TEC of graphene is expected to be linear [32], the strain dependence around 100 K is presumably induced by an anomaly around 120 K in the thermal expansion of the Si substrate [50].

Second, the strain at 300 K in the ^{12}C isotope layer of T-2LG is small, whereas the strain in the ^{13}C isotope layer is much higher. This large difference is related to the different interfaces of the two layers. Whereas the ^{13}C graphene bottom layer is in direct contact with the SiO_2/Si substrate, the ^{12}C graphene top layer is in contact with the ^{13}C graphene bottom layer.

High-temperature Raman measurements on graphene have shown that the first heating cycle resulted in a graphene layer's slipping on the top of the substrate, whereas the interaction was found to be much more stable after further heating cycles [23,24]. This suggests that during the thermal annealing before the low-temperature measurements, the graphene layer becomes stabilized, which, together with the formed wrinkles, prevents it from extensive slipping during heating/cooling cycles performed in this study.

The ^{12}C top-layer graphene is, however, in contact with the ^{13}C bottom layer. The more relaxed graphene top layer is then a consequence of the weak van der Waals interactions between the two graphene layers, which enables the top layer to move more freely, as shown by Kalbac *et al.* [34].

In addition to the anharmonic phonon contribution, the isotope composition plays an important role in material properties such as specific heat, thermal expansion, and carrier transport properties [51]. The TEC of the ^{13}C isotope is estimated using the scaling relation [52,53] $a_{13}(T) \simeq a_{12}(T\sqrt{m_{13}/m_{12}}) - \Delta a_0$, where a_{12}, a_{13}, m_{12}, and m_{13} are the lattice parameters and the masses of the ^{12}C and ^{13}C graphene layers, respectively, and Δa_0 is the difference in lattice constants at low temperatures. For the ^{12}C graphene layer, the temperature dependence of the calculated lattice parameter [54] is used and we assume that the difference in lattice parameters between ^{12}C and ^{13}C graphene is approximately the same as that between ^{12}C and ^{13}C diamond [55] (5×10^{-4} Å at 300 K). From this, we can expect that both isotopically labeled graphene layers have approximately the same TEC.

Although the strain in the ^{12}C graphene top layer and ^{13}C graphene bottom layer are not identical at 300 K, the strain in both layers behaves the same as in ^{13}C-1LG the temperature is decreased. This suggests that during the annealing both layers become stabilized with respect to each other. When the temperature is subsequently varied, the same amount of strain is induced in both the bottom and the top layers.

Recent experiments have suggested that the FWHM of the 2D mode is an indication of strain inhomogeneities that are much smaller than the size of the laser spot (<500 nm) [20,43,56]. Figure 5(f) shows that the temperature dependences of the median FWHM of the ^{12}C graphene top layer and ^{13}C graphene bottom layer are different. Whereas the median FWHM of the ^{12}C $2D_1$ peak increases by 3 cm^{-1}, the median FWHM of the ^{13}C $2D_1$ peak increases by 6 cm^{-1} when the sample is cooled from 300 to 200 K. This suggests that on a "local" scale, more strain variation is induced in the bottom layer, which is in contact with the substrate, than in the top layer. The temperature dependence of the locally induced strain is also clearly visible in the median FWHM of the ^{13}C-1LG, as shown in Fig. 3(f). Thus, the influence of the bulk response of the substrate to the changes of the temperature plays an important role in thermally induced changes in the topography of the graphene monolayer/bilayer and must be

carefully considered in all experiments where the samples undergo significant thermal changes.

Figures 3(d) and 5(d) show the median FWHM of the G_1 mode. Although the doping level of the ^{13}C bottom layer is higher than that of the ^{12}C top layer [see Fig. 6(c)], the median FWHM of the ^{13}C bottom layer is almost the same as that of the ^{12}C top layer. An increase in the FWHM of the graphene layers can be caused by charge puddles/inhomogeneities that are present in the SiO_2/Si substrate.

Figure 6(c) shows that when the sample is cooled from 300 to 200 K, an increase in the doping is observed for both the ^{13}C and the ^{12}C graphene layers. Decreasing the temperature further does not reveal a clear relation between the doping and the temperature.

Another remarkable difference in the induced doping in the bottom versus the top layer of the graphene bilayer is that the doping level in the bottom layer is much higher than that in the graphene top layer. The graphene bottom layer thus provides an effective screening of the induced doping from the SiO_2/Si substrate, which is also observed when graphene is placed on a thin layer of MoS_2 [57] or hBN [58].

V. CONCLUSION

To conclude, we have measured temperature-dependent maps of Raman spectra of mono- and isotopically labeled bilayer graphene. The large number of spectra collected in the Raman maps allows us to use correlation analysis to distinguish the influence of both the strain and the doping on the Raman shift of the active modes of graphene and provide sufficient statistics to draw conclusions.

The strain, which is induced during growth and annealing, is much higher in the bottom layer, which is in contact with the substrate, than in the top layer, which is in contact with the graphene bottom layer only. However, the temperature dependence of both the bottom and the top layers is similar and follows well the thermal expansion of the SiO_2/Si substrate.

However, we find that more strain on length scales much smaller than the laser spot is induced in the graphene layer that is in contact with the SiO_2/Si substrate. In addition, a clear temperature dependence of the doping is present.

These measurements imply that doping and, especially, strain should be taken into account when analyzing transport measurements on graphene mono- and bilayers that have undergone large temperature cycles.

ACKNOWLEDGMENTS

The work was supported by the Czech Science Foundation (Grant No. 15-01953S) and ERC-CZ:LL1301. Experiments were performed at the Magnetism and Low Temperatures Laboratories, Prague (see http://mltl.eu), which is supported within the program Czech Research Infrastructures (Project No. LM2011025).

[1] A. H. Castro Neto, F. Guinea, N. M. R. Peres, K. S. Novoselov, and A. K. Geim, Rev. Mod. Phys. **81**, 109 (2009).
[2] F. Schwierz, Nat. Nano **5**, 487 (2010).
[3] F. Bonaccorso, Z. Sun, T. Hasan, and A. C. Ferrari, Nat. Photon. **4**, 611 (2010).
[4] P. Avouris, Nano Lett. **10**, 4285 (2010).
[5] A. N. Grigorenko, M. Polini, and K. S. Novoselov, Nat. Photon. **6**, 749 (2012).
[6] R. J. Young, I. A. Kinloch, L. Gong, and K. S. Novoselov, Compos. Sci. Technol. **72**, 1459 (2012).
[7] A. A. Balandin, Nat. Mater. **10**, 569 (2011).
[8] K. S. Novoselov, V. I. Fal'ko, L. Colombo, P. R. Gellert, M. G. Schwab, and K. Kim, Nature **490**, 192 (2012).
[9] S. Das Sarma, S. Adam, E. H. Hwang, and E. Rossi, Rev. Mod. Phys. **83**, 407 (2011).
[10] F. Guinea, M. I. Katsnelson, and A. K. Geim, Nat. Phys. **6**, 30 (2010).
[11] N. Levy, S. A. Burke, K. L. Meaker, M. Panlasigui, A. Zettl, F. Guinea, A. H. C. Neto, and M. F. Crommie, Science **329**, 544 (2010).
[12] M. Mucha-Kruczyński, I. L. Aleiner, and V. I. Fal'ko, Phys. Rev. B **84**, 041404 (2011).
[13] E. Mariani, A. J. Pearce, and F. von Oppen, Phys. Rev. B **86**, 165448 (2012).
[14] C. Casiraghi, S. Pisana, K. S. Novoselov, A. K. Geim, and A. C. Ferrari, Appl. Phys. Lett. **91**, 233108 (2007).
[15] S. Berciaud, S. Ryu, L. E. Brus, and T. F. Heinz, Nano Lett. **9**, 346 (2008).
[16] M. Ishigami, J. H. Chen, W. G. Cullen, M. S. Fuhrer, and E. D. Williams, Nano Lett. **7**, 1643 (2007).
[17] K. R. Knox, S. Wang, A. Morgante, D. Cvetko, A. Locatelli, T. O. Mentes, M. A. Niño, P. Kim, and R. M. Osgood, Phys. Rev. B **78**, 201408 (2008).
[18] U. Stberl, U. Wurstbauer, W. Wegscheider, D. Weiss, and J. Eroms, Appl. Phys. Lett. **93**, 051906 (2008).
[19] V. Geringer, M. Liebmann, T. Echtermeyer, S. Runte, M. Schmidt, R. Rückamp, M. C. Lemme, and M. Morgenstern, Phys. Rev. Lett. **102**, 076102 (2009).
[20] N. J. G. Couto, D. Costanzo, S. Engels, D.-K. Ki, K. Watanabe, T. Taniguchi, C. Stampfer, F. Guinea, and A. F. Morpurgo, Phys. Rev. X **4**, 041019 (2014).
[21] W. Zhu, T. Low, V. Perebeinos, A. A. Bol, Y. Zhu, H. Yan, J. Tersoff, and P. Avouris, Nano Lett. **12**, 3431 (2012).
[22] A. T. N'Diaye, R. van Gastel, A. J. Martínez-Galera, J. Coraux, H. Hattab, D. Wall, F.-J. M. zu Heringdorf, M. H. von Hoegen, J. M. Gómez-Rodríguez, B. Poelsema, C. Busse, and T. Michely, New J. Phys. **11**, 113056 (2009).
[23] M. Kalbac, O. Frank, and L. Kavan, Chem. Eur. J. **18**, 13877 (2012).
[24] D. Yoon, Y.-W. Son, and H. Cheong, Nano Lett. **11**, 3227 (2011).
[25] A. Das, S. Pisana, B. Chakraborty, S. Piscanec, S. K. Saha, U. V. Waghmare, K. S. Novoselov, H. R. Krishnamurthy, A. K. Geim, A. C. Ferrari, and A. K. Sood, Nat. Nanotechnol. **3**, 210 (2008).

[26] A. Das, B. Chakraborty, S. Piscanec, S. Pisana, A. K. Sood, and A. C. Ferrari, Phys. Rev. B **79**, 155417 (2009).
[27] T. M. G. Mohiuddin, A. Lombardo, R. R. Nair, A. Bonetti, G. Savini, R. Jalil, N. Bonini, D. M. Basko, C. Galiotis, N. Marzari, K. S. Novoselov, A. K. Geim, and A. C. Ferrari, Phys. Rev. B **79**, 205433 (2009).
[28] J. Zabel, R. R. Nair, A. Ott, T. Georgiou, A. K. Geim, K. S. Novoselov, and C. Casiraghi, Nano Lett. **12**, 617 (2012).
[29] J. E. Lee, G. Ahn, J. Shim, Y. S. Lee, and S. Ryu, Nat. Commun. **3**, 1024 (2012).
[30] I. Calizo, A. A. Balandin, W. Bao, F. Miao, and C. N. Lau, Nano Lett. **7**, 2645 (2007).
[31] P. Giura, N. Bonini, G. Creff, J. B. Brubach, P. Roy, and M. Lazzeri, Phys. Rev. B **86**, 121404 (2012).
[32] N. Bonini, M. Lazzeri, N. Marzari, and F. Mauri, Phys. Rev. Lett. **99**, 176802 (2007).
[33] J. Lin, L. Guo, Q. Huang, Y. Jia, K. Li, X. Lai, and X. Chen, Phys. Rev. B **83**, 125430 (2011).
[34] M. Kalbac, H. Farhat, J. Kong, P. Janda, L. Kavan, and M. S. Dresselhaus, Nano Lett. **11**, 1957 (2011).
[35] O. Frank, L. Kavan, and M. Kalbac, Nanoscale **6**, 6363 (2014).
[36] A. S. Reina, H. Son, L. Jiao, B. Fan, M. S. Dresselhaus, Z. Liu, and J. Kong, J. Phys. Chem. C **112**, 17741 (2008).
[37] See Supplemental Material at http://link.aps.org/supplemental/10.1103/PhysRevB.92.125437 for comments on thed statistical analysis method used to analyze Raman maps and the calibration of the confocal Raman microscope at 10 K.
[38] W. Fang, A. L. Hsu, R. Caudillo, Y. Song, A. G. Birdwell, E. Zakar, M. Kalbac, M. Dubey, T. Palacios, M. S. Dresselhaus, P. T. Araujo, and J. Kong, Nano Lett. **13**, 1541 (2013).
[39] J. E. Weis, S. D. Costa, O. Frank, and M. Kalbac, Phys. Status Solidi B **251**, 2505 (2014).
[40] M. Kalbac, V. Vales, and J. Vejpravova, RSC Adv. **4**, 60929 (2014).
[41] J. Vejpravova, B. Pacakova, J. Endres, A. Mantlikova, T. Verhagen, V. Vales, O. Frank, and M. Kalbac, Sci. Rep. **5**, 15061 (2015), doi:10.1038/srep15061.
[42] Q. Li, H. Chou, J.-H. Zhong, J.-Y. Liu, A. Dolocan, J. Zhang, Y. Zhou, R. S. Ruoff, S. Chen, and W. Cai, Nano Lett. **13**, 486 (2013).
[43] O. Frank, J. Vejpravova, V. Holy, L. Kavan, and M. Kalbac, Carbon **68**, 440 (2014).
[44] K. G. Lyon, G. L. Salinger, C. A. Swenson, and G. K. White, J. Appl. Phys. **48**, 865 (1977).
[45] M. S. Dresselhaus, A. Jorio, M. Hofmann, G. Dresselhaus, and R. Saito, Nano Lett. **10**, 751 (2010).
[46] D. L. Mafra, G. Samsonidze, L. M. Malard, D. C. Elias, J. C. Brant, F. Plentz, E. S. Alves, and M. A. Pimenta, Phys. Rev. B **76**, 233407 (2007).
[47] A. T. Apostolov, I. N. Apostolova, and J. M. Wesselinowa, J. Phys.: Condens. Matter **24**, 235401 (2012).
[48] M. Kalbac, O. Lehtinen, A. V. Krasheninnikov, and J. Keinonen, Adv. Mater. **25**, 1004 (2013).
[49] G. Froehlicher and S. Berciaud, Phys. Rev. B **91**, 205413 (2015).
[50] J. S. Shah and M. Straumanis, Solid State Commun. **10**, 159 (1972).
[51] M. Cardona and M. L. W. Thewalt, Rev. Mod. Phys. **77**, 1173 (2005).
[52] A. Zhernov, Phys. Solid State **40**, 1658 (1998).
[53] H.-C. Wille, Y. V. Shvyd'ko, E. Gerdau, M. Lerche, M. Lucht, H. D. Rüter, and J. Zegenhagen, Phys. Rev. Lett. **89**, 285901 (2002).
[54] K. V. Zakharchenko, M. I. Katsnelson, and A. Fasolino, Phys. Rev. Lett. **102**, 046808 (2009).
[55] H. Holloway, K. C. Hass, M. A. Tamor, T. R. Anthony, and W. F. Banholzer, Phys. Rev. B **44**, 7123 (1991).
[56] C. Neumann, S. Reichardt, M. Drögeler, K. Watanabe, T. Taniguchi, B. Beschoten, S. V. Rotkin, and C. Stampfer, arXiv:1406.7771 [cond-mat.mes-hall].
[57] C.-P. Lu, G. Li, K. Watanabe, T. Taniguchi, and E. Y. Andrei, Phys. Rev. Lett. **113**, 156804 (2014).
[58] C. R. Dean, A. F. Young, I. Meric, C. Lee, L. Wang, S. Sorgenfrei, K. Watanabe, T. Taniguchi, P. Kim, K. L. Shepard, and J. Hone, Nat. Nano **5**, 722 (2010)